Discussion on the Origin of the Strength of Phasor Quaternion Self-Organizing Map

Yicheng Song* and Akira Hirose†
* The University of Tokyo, Tokyo, Japan
E-mail: song_yicheng@eis.t.u-tokyo.ac.jp
† The University of Tokyo, Tokyo, Japan
E-mail: ahirose@ee.t.u-tokyo.ac.jp

***Abstract*—Previously we proposed a ground penetrating radar (GPR) system employing the phasor quaternion self-organizing map (PQSOM) to deal with phasor quaternion (PQ) feature vectors extracted from scattering matrices. It performs unsupervised grouping to achieve visualization. Compared with conventional complex-valued self-organizing maps (CSOM) and quaternion self-organizing map (QSOM), PQSOM has better grouping performance. In this paper, we investigate the origin of the strength of PQSOM. We discuss the advantages of using PQ vectors as feature vectors from a extracted data perspective, and then analyze how update rules of PQSOM effectively use PQ vectors to achieve better visualization. Our analysis is verified by the experimental results.**

I. Introduction

Ground penetrating radar (GPR)-based underground visualization is a field with a wide range of demands and various applications. Visualization of anti-personnel plastic landmines is a relatively difficult task as landmines are small, non-metallic and prone to the influence of debris, rubble, etc. Sometimes the visualization is performed for raw data by employing a fixed signal processing [1]–[3]. Other cases adopt adaptive methods such as neural networks to utilize the information in the data effectively [4]–[6]. One of the effective methods is to achieve landmine imaging through complex-valued self-organizing map (CSOM), a self-organizing algorithm [7]–[9]. The CSOM [8] uses the spatial and frequency correlation of scattering parameters for self-organization and grouping. The experimental results show that for some difficult situations, CSOM has problems such as unclear landmine boundaries and landmine shape distortion.

Recently, the authors' group has proposed a polarization feature extraction method based on the scattering matrix [10], [11]. We analyzed its effectiveness at the theoretical level, and also applied it to the processing of synthetic aperture radar (SAR) data to show its high performance. Another paper has improved this feature extraction method by adding phase information to define a new form called phasor quaternion (PQ) [12]. Phasor quaternion neural network (PQNN) based on PQ shows good performance in the residue removal task of SAR data.

Based on all of the above, we proposed a PQ-based algorithm called phasor quaternion self-organizing map (PQSOM) [13], [14]. Through experiments, we found that PQSOM overcomes the shortcomings of CSOM and has better performance than not only CSOM but also quaternion self-organizing map (QSOM). In this paper, we investigate the origin of the strength of PQSOM. We discuss the advantages of using PQ vectors as feature vectors from a extracted data perspective, and then analyze how update rules of PQSOM effectively use PQ vectors to achieve better visualization. Through experiments, our conclusions are verified.

This paper is organized as follows. Section II briefly describes the structure of our system and the feature extraction method of PQSOM. Section III reviews the dynamics of PQSOM and discuss the origin of the strength of PQSOM. Section IV summarizes our discussion and makes conclusions.

II. System Structure and Feature Extraction

A. Overall System Structure

The structure of the PQSOM-based GPR system is described as follows. First, we obtain multiple frequency scattering matrices of each spatial measuring point as raw data. Second, we extract feature vectors from the raw data for a PQSOM to self-organize. After self-organization, we feed the data to the PQSOM again for grouping the feature vectors, and then plot the segmented image in the real space.

B. Feature Extraction

The feature extraction method of PQSOM follows the basic idea of Ref. [12]. Simply speaking, the method consists of two steps.

First, we derive Poincare vectors for each local window with some incident waves assumed. To be more specific, for a fixed local window and a fixed frequency, we have some scattering matrices included in the window. Then, for an assumed incident wave combined with those matrices, we can get a Poincare vector. For PQSOM, we assume six different incident waves of six polarization states: Horizontal (H), Vertical (V), $+45°$, $-45°$, Left Circular (LC), Right Circular (RC) for each local window. Hence, for a local window, we get six Poincare vectors.

Each incident wave can be expressed by its unit Jones vector $\left[E_{\mathrm{H}}^{\mathrm{i}}\ E_{\mathrm{V}}^{\mathrm{i}}\right]^{\mathrm{T}}$ (T: transpose) shown in Table I, where $E_{\mathrm{H}}^{\mathrm{i}}$ and $E_{\mathrm{V}}^{\mathrm{i}}$ stand for horizontal and vertical components, respectively. Then, for an incident wave, the scattered wave $[E_{\mathrm{H}}^{\mathrm{r}}\ E_{\mathrm{V}}^{\mathrm{r}}]^{\mathrm{T}}$ is

TABLE I
UNIT JONES VECTORS OF DIFFERENT POLARIZATION STATES

Incident wave	Polarization state					
	H	V	$+45^\circ$	-45°	LC	RC
$\begin{bmatrix} E_{\mathrm{H}}^{\mathrm{i}} \\ E_{\mathrm{V}}^{\mathrm{i}} \end{bmatrix}$	$\begin{bmatrix} 1 \\ 0 \end{bmatrix}$	$\begin{bmatrix} 0 \\ 1 \end{bmatrix}$	$\begin{bmatrix} \frac{1}{\sqrt{2}} \\ \frac{1}{\sqrt{2}} \end{bmatrix}$	$\begin{bmatrix} -\frac{1}{\sqrt{2}} \\ \frac{1}{\sqrt{2}} \end{bmatrix}$	$\begin{bmatrix} \frac{1}{\sqrt{2}} \\ j\frac{1}{\sqrt{2}} \end{bmatrix}$	$\begin{bmatrix} \frac{1}{\sqrt{2}} \\ -j\frac{1}{\sqrt{2}} \end{bmatrix}$

obtained by

$$\begin{bmatrix} E_{\mathrm{H}}^{\mathrm{r}} \\ E_{\mathrm{V}}^{\mathrm{r}} \end{bmatrix} = \begin{bmatrix} S_{\mathrm{HH}} & S_{\mathrm{HV}} \\ S_{\mathrm{VH}} & S_{\mathrm{VV}} \end{bmatrix} \begin{bmatrix} E_{\mathrm{H}}^{\mathrm{i}} \\ E_{\mathrm{V}}^{\mathrm{i}} \end{bmatrix}. \tag{1}$$

Further the Jones coherency matrix $\mathbf{J}$ is calculated as

$$\mathbf{J} = \begin{bmatrix} J_{\mathrm{HH}} & J_{\mathrm{HV}} \\ J_{\mathrm{VH}} & J_{\mathrm{VV}} \end{bmatrix} = \begin{bmatrix} \langle E_{\mathrm{H}}^{\mathrm{r}} E_{\mathrm{H}}^{\mathrm{r}^*} \rangle & \langle E_{\mathrm{H}}^{\mathrm{r}} E_{\mathrm{V}}^{\mathrm{r}^*} \rangle \\ \langle E_{\mathrm{V}}^{\mathrm{r}} E_{\mathrm{H}}^{\mathrm{r}^*} \rangle & \langle E_{\mathrm{V}}^{\mathrm{r}} E_{\mathrm{V}}^{\mathrm{r}^*} \rangle \end{bmatrix} \tag{2}$$

where $\langle \cdot \rangle$ indicates spatial average, $\cdot^*$ denotes the conjugate of a complex number. From the Jones coherency matrix, the averaged Stokes vector $[\langle g_0 \rangle \ \langle g_1 \rangle \ \langle g_2 \rangle \ \langle g_3 \rangle]^{\mathrm{T}}$ is calculated as

$$\begin{bmatrix} \langle g_0 \rangle \\ \langle g_1 \rangle \\ \langle g_2 \rangle \\ \langle g_3 \rangle \end{bmatrix} = \begin{bmatrix} J_{\mathrm{HH}} + J_{\mathrm{VV}} \\ J_{\mathrm{HH}} - J_{\mathrm{VV}} \\ J_{\mathrm{HV}} + J_{\mathrm{VH}} \\ j(J_{\mathrm{HV}} - J_{\mathrm{VH}}) \end{bmatrix} \tag{3}$$

where j denotes the imaginary unit. The components $\langle g_0 \rangle$, $\langle g_1 \rangle$, $\langle g_2 \rangle$ and $\langle g_3 \rangle$ mean total power, degree of horizontal polarization, degree of $+45^\circ$ polarization and degree of LC polarization, respectively. The average Stoke vector indicates the polarization state information of the scattered wave. It can be expressed as a point on or in the unit sphere called Poincare sphere. The position coordinate of the point is

$$\left(\frac{\langle g_1 \rangle}{\langle g_0 \rangle} \quad \frac{\langle g_2 \rangle}{\langle g_0 \rangle} \quad \frac{\langle g_3 \rangle}{\langle g_0 \rangle} \right). \tag{4}$$

We call it Poincare vector.

Second, we combine the Poincare vector and phase information of S_{HH} to get a new form called phasor quaternion defined as

$$\mathbf{p} = \mathbf{p}^q \mathbf{p}^p := \left(0 \quad \frac{\langle g_1 \rangle}{\langle g_0 \rangle} \quad \frac{\langle g_2 \rangle}{\langle g_0 \rangle} \quad \frac{\langle g_3 \rangle}{\langle g_0 \rangle} \right) e^{j \arg\{S_{\mathrm{HH}}\}} \tag{5}$$

where $\mathbf{p}^q$ is the quaternion part representing polarization and $\mathbf{p}^p$ is the phasor part corresponding to the phase part. Phasor quaternion was first introduced in phasor quaternion neural network for removing artificial residues of SAR data [12].

III. PQSOM

A. Dynamics of PQSOM

Algorithm 1 shows the processing flow of PQSOM. At the beginning, we initialize each weight vector. Then we feed a input vector set to the PQSOM for several epochs. For an input vector, we have to find the Best Match Unit (BMU) at first. This is called competition stage. In other words, we need to find a neuron whose weight vector is the closest to the input vector. Then we update the weight vectors of BMU and its neighbors. This is called adaptation stage. After self-organization, we feed the input vector set to the PQSOM again to group the input vectors and plot the segmented image to show the result.

Algorithm 1: PQSOM Algorithm

Input: a set of input vectors $\{\boldsymbol{p}(x,y)\}$, where $x \in \{1,...,X\}$ and $y \in \{1,...,Y\}$; class number C; epoch number E.

Output: a set of classes of input vectors $\{c_{(x,y)}\}$.

% Initialization:
randomly initialize each $\boldsymbol{w}_c = \boldsymbol{w}_c(0)$
% Self-organization:
for $t = 1$ *to* $T = XYE$ **do**
  % Competition:
  find the best matching unit (BMU)
   $\hat{c} = \arg\min_{c \in C} d(\boldsymbol{p}(t), \boldsymbol{w}_c(t))$
  % Adaptation:
  update the weights of the BMU $\hat{c}$ ($\boldsymbol{w}_{\hat{c}}$) and its neighbors
end
% Grouping:
group input vectors with self-organized PQSOM
 $c_{(x,y)} = \arg\min_{c \in C} d(\boldsymbol{p}(x,y), \boldsymbol{w}_c(T))$

In the adaptation stage, we update the weights of the BMU and its neighbors of the Ring-PQSOM as follows. For the quaternion part vector $\boldsymbol{w}_{\hat{c}}^q = [\mathbf{w}_{\hat{c}\,km}^q]$ and phase $\boldsymbol{\phi}_{\hat{c}} = [\phi_{\hat{c}\,km}]$ in the phasor part vector $\boldsymbol{w}_{\hat{c}}^p (= [\mathbf{w}_{\hat{c}\,km}^p]) = \exp(j\boldsymbol{\phi}_{\hat{c}}) = [\exp(j\boldsymbol{\phi}_{\hat{c}\,km})]$ $(1 \le k \le K, 1 \le m, d \le M)$ of the BMU, we determine the update rule using quaternion part vector $\boldsymbol{p}^q(t) = [\mathbf{p}_{km}^q(t)]$ and phasor part vector $\boldsymbol{p}^p(t) = [\mathbf{p}_{km}^p(t)]$ of the t-th input vector $\boldsymbol{p}(t)$ as

$$\begin{aligned} \mathbf{w}_{\hat{c}\,km}^q(t+1) &= \mathbf{w}_{\hat{c}\,km}^q(t) \\ &\quad + \alpha(t)(\mathbf{p}_{km}^q(t) - \mathbf{w}_{\hat{c}\,km}^q(t)) && (6) \\ \phi_{\hat{c}\,km}(t+1) &= \phi_{\hat{c}\,km}(t) - \alpha(t)(\textstyle\sum_d |\mathbf{p}_{kd}^q(t)|) \\ &\quad \cdot \sin(\phi_{\hat{c}\,km}(t) - \theta_{km}(t)) && (7) \\ \alpha(t) &= (1 - \frac{t}{T})\alpha_0 && (8) \\ \phi_{\hat{c}\,km}(t) &= \arg\{\mathbf{w}_{\hat{c}\,km}^p(t)\} && (9) \\ \theta_{km}(t) &= \arg\{\mathbf{p}_{km}^p(t)\} && (10) \end{aligned}$$

where α_0 denotes learning coefficient for the BMU and T is the total self-organization time.

For the BMU's neighbors,

$$\begin{aligned} \mathbf{w}_{\hat{c}\pm1\,km}^q(t+1) &= \mathbf{w}_{\hat{c}\pm1\,km}^q(t) \\ &\quad + \beta(t)(\mathbf{p}_{km}^q(t) - \mathbf{w}_{\hat{c}\pm1\,km}^q(t)) && (11) \\ \phi_{\hat{c}\pm1\,km}(t+1) &= \phi_{\hat{c}\pm1\,km}(t) - \beta(t)(\textstyle\sum_d |\mathbf{p}_{kd}^q(t)|) \\ &\quad \cdot \sin(\phi_{\hat{c}\pm1\,km}(t) - \theta_{km}(t)) && (12) \\ \beta(t) &= (1 - \frac{t}{T})\beta_0 && (13) \\ \phi_{\hat{c}\pm1\,km}(t) &= \arg\{\mathbf{w}_{\hat{c}\pm1\,km}^p(t)\} && (14) \end{aligned}$$

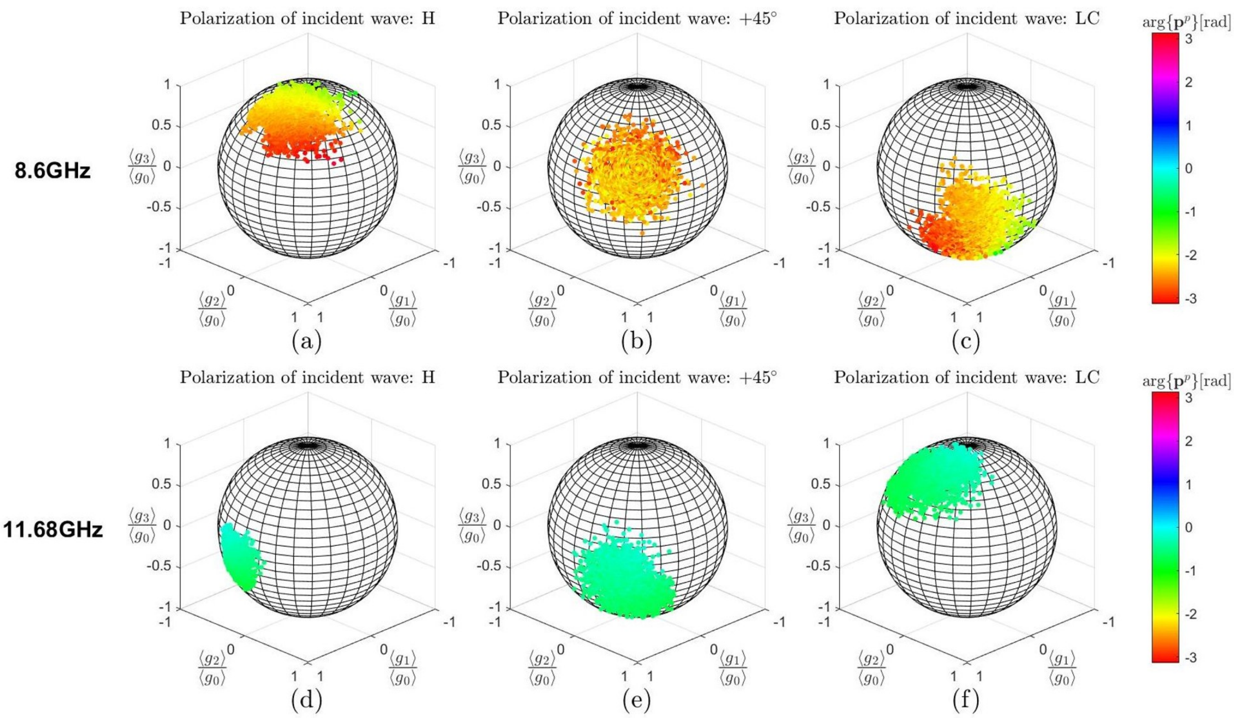

Fig. 1. Phasor quaternions for incident waves of (a) H, (b) $+45°$, as well as (c) LC at 8.6GHz, (d) H, (e) $+45°$, (f) LC at 11.68GHz, respectively, where the quaternion part of each PQ is plotted on or in the unit sphere (Poincare sphere), and the phase of phasor part is represented by color.

where $\beta_0(<\alpha_0)$ denotes learning coefficient for the neighbors.

B. Coordinated Change Feature

Unlike conventional CSOM and QSOM, PQSOM uses PQ vectors as feature vectors. PQ takes both polarization state and phase information into account, and considers them as a whole. The polarization and phase have a coordinated change feature shown in Figure 1. Figure 1 shows the phasor quaternions for three polarized incident waves of H, $+45°$, LC at 8.6GHz and 11.68GHz. The quaternion part of each PQ is plotted on or in the unit sphere (Poincare sphere), and the phase of phasor part is represented by color. First, we can get the following fact by observing Figure 1. Regardless of the frequency or incident wave, for those points with similar polarization, their phase is also similar. According to the electromagnetic wave theory, for the points in landmine area, the polarization states of the scattered waves should be similar among them but different from polarization states of points in the non-landmine area. Based on the above facts, we can conclude that the phase of points in the landmine area is similar and different from that in non-landmine area. We call this feature coordinated change. Intuitively speaking, when the polarization (quaternion part $\mathbf{p}^q$) gradually changes, the phase (phasor part $\mathbf{p}^p$) will gradually change along with it. For most of frequencies and incident waves, this phenomenon is observed. For the rest, this phenomenon is not so obvious, such as Figure 1 (b).

This observation implies that polarization and phase contain related information. For a neural network (NN), its ability can be enhanced by properly preparing different types of information representing even for identical entities. SOM is a type of NN. Hence, the self-organization ability of PQSOM is enhanced by combining polarization with phase information into PQ form as input. In addition, for each PQ vector, we consider six different incident waves. This process also enhances the self-organization ability of PQSOM by introducing a variety in the scattering feature representation. The grouping results below support our thought.

C. Design of Update Rules

In order to make full use of the valid information of PQ, the design of update rules of PQSOM is the key point. Since phasor quaternion is a new type of number, not two separate parts, we need to reflect its integrity. We get the idea from CSOM to design update rules. For quaternion part, we update it in the same way as CSOM without phase. For phasor part, the update rule of CSOM is derived from the partial derivative of the loss function [9]. We follow the same steps to derive the update rule for PQSOM except for substituting the norm of quaternion part for the amplitude of complex number. Then, in the phasor part update rules (7) and (12)

$$\begin{aligned}\phi_{\hat{c}\,km}(t+1) &= \phi_{\hat{c}\,km}(t) - \alpha(t)(\textstyle\sum_d |\mathbf{p}^q_{kd}(t)|) \\ &\quad \cdot \sin(\phi_{\hat{c}\,km}(t) - \theta_{km}(t)) \\ \phi_{\hat{c}\pm 1\,km}(t+1) &= \phi_{\hat{c}\pm 1\,km}(t) - \beta(t)(\textstyle\sum_d |\mathbf{p}^q_{kd}(t)|) \\ &\quad \cdot \sin(\phi_{\hat{c}\pm 1\,km}(t) - \theta_{km}(t)),\end{aligned}$$

the norm of quaternion part $\sum_d |\mathbf{p}^q_{kd}(t)|$ is also considered. This shows that, akin to CSOM, the norm of PQ can also influence the phase update. Since this update method emphasizes the fact that PQ is an entity as a whole, the related useful information between the quaternion part and the phasor part can be strengthened during the phase update process, which in turn makes the self-organization ability of PQSOM enhanced. Hence, our design makes good use of the coordinated change feature between polarization and phase shown in the extracted data. Therefore, PQSOM should have better visualization performance. From the experimental results, this design plays its expected role.

D. Experimental Results

Figure 2 shows the grouping results of CSOM, QSOM, and PQSOM. The boundary of buried landmine is shown as dashed circle in the figure. Each color represents a class (i.e., a neuron). It is obvious that PQSOM has the best result. The boundary of the possible landmine area is clear, and the shape of the area is almost the same as real landmine shape. The experimental results validate the previous analysis and discussions. The use of PQ vectors as feature vectors and the corresponding update method can indeed improve the visualization performance of PQSOM.

We also compare two distance functions, namely, Euclidean metric and inner product. From the results, inner product has a higher performance since there is no possible landmine area in the background, and the background grouping is more uniform. Since PQSOM is an unsupervised learning algorithm, here we do not identify which class the landmine belongs to. However, we can adaptively identify the landmine class by evaluating the total degree of conformity of Ring-SOM weights. For details, please refer to Ref. [15]. In addition, the lowest DoP of the raw data is about 0.8 in the experiment, which means that for some frequencies and locations, the scattered waves are partially polarized. The grouping results of PQSOM imply that PQSOM also utilizes the DoP information effectively. Therefore, PQSOM should be able to achieve good grouping even for relatively low DoP data.

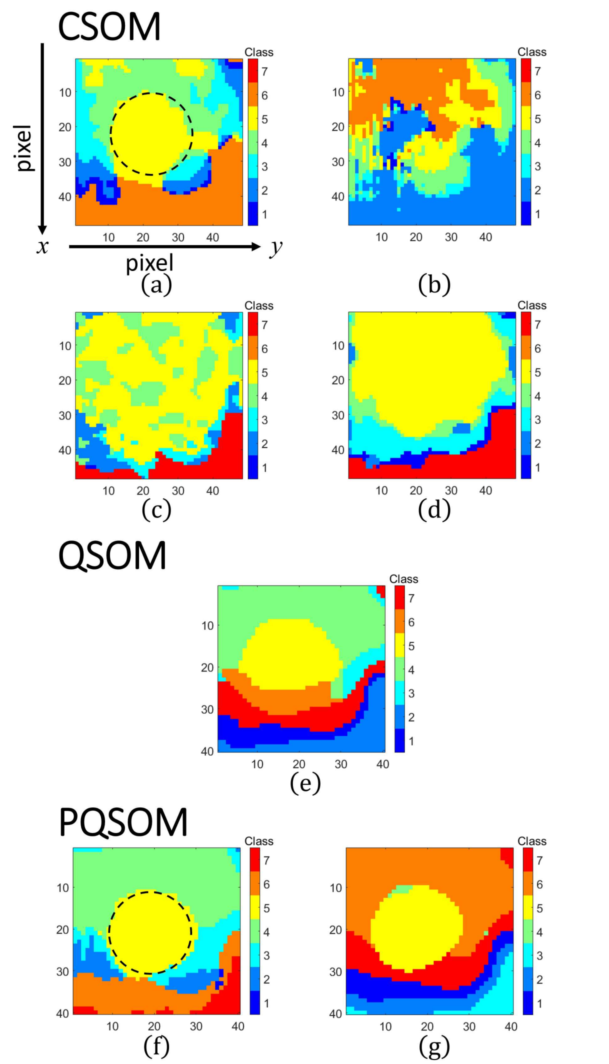

Fig. 2. Grouping results of CSOM for (a) S_{HH}, (b) S_{HV}, (c) S_{VH} and (d) S_{VV} as raw data, QSOM with (e) Euclidean metric as distance function, as well as PQSOM with (f) Euclidean metric and (g) inner product as distance functions [13].

IV. Conclusions

Previously, we proposed the PQSOM and applied it to the detection of anti-personnel plastic landmines. The visualization results of PQSOM are better than conventional CSOM and QSOM. In this paper, we discussed the origin of the strength of PQSOM. Through observing the data, we found that the phase and polarization information of the data have the coordinated change feature. Based on this feature, the use of PQ feature vectors can effectively enhance the self-organization ability of PQSOM. Then we looked at the details of the update rules of PQSOM. The design of phasor part update rules can effectively utilize the coordinated change feature of PQ.

To sum up, there are three reasons that make PQSOM more effective:

1 Polarization (quaternion part) and phase (phasor part) are respective counterparts, which means that they contain related useful information. At the feature extraction stage, input vectors of PQSOM contain more information than CSOM or QSOM does. Hence, PQSOM is more likely to work better than QSOM and CSOM.

2 We do not simply considering phase as an additional dimension of polarization by adding it to the quaternion part to get a five-dimensional real vector. According to the coordinated change feature between them, we use the form of phasor quaternion to turn them into a new number. Then in the self-organizing process, the quaternion part is used in the phase update rules. Through this design, we expect that the related useful information they share can be strengthened, rather than just let them update independently without influencing

each other. Therefore, we can effectively enhance the self-organization capability of PQSOM, and thus achieve better visualization.

3 We designed the phase update rules by following the successful experience of CSOM, which guarantees the convergence of the algorithm and basic performance.

We validated our theoretical-level analysis through experiments. Experimental results show that, compared with the conventional CSOM and QSOM, the PQSOM has better visualization performance. Our analysis also implies that PQ, a new feature extraction approach, can be widely used in topics related to electromagnetic waves. We will further improve the theory of PQ-related algorithms and expand the scope of application.

Acknowledgment

This work was supported in part by JSPS KAKENHI under Grant No.18H04105, and in part by the Cooperative Research Project Program of the Research Institute of Electrical Communication (RIEC), Tohoku University.

References

[1] T. P. Montoya and G. S. Smith, “Land mine detection using a ground penetrating radar based on resistively loaded vee dipoles,” *IEEE Transactions on Antennas and Propagation,* vol. 47, no. 12, pp. 1795–1806, 1999.

[2] M. Sato, Y. Hamada, X. Feng, F. N. Kong, Z. F. Zeng, and G. Y. Fang, “GPR using an array antenna for landmine detection,” *Near Surface Geophysics,* vol. 2, no. 1, pp. 7–13, 2004.

[3] M. Kim, S. Kim, J. Hahm, and S. Choi, “GPR image enhancement based on frequency shifting and histogram dissimilarity,” *IEEE Geoscience and Remote Sensing Letters,* vol. 15, no. 5, pp. 684–688, 2018.

[4] C. C. Yang and N. K. Bose, “Landmine detection and classification with complex-valued hybrid neural network using scattering parameters dataset,” *IEEE Transactions on Neural Networks,* vol. 16, no. 3, pp. 743–753, 2005.

[5] S. E. Yuksel, J. Bolton, and P. Gader, “Multiple-instance hidden Markov models with applications to landmine detection,” *IEEE Transactions on Geoscience and Remote Sensing,* vol. 53, no. 12, pp. 6766–6775, 2015.

[6] R. Karlina and M. Sato, “Model-based compressive sensing applied to landmine detection by GPR,” *IEICE Transactions on Electronics,* vol. 99, no. 1, pp. 44-51, 2016.

[7] T. Hara and A. Hirose, “Plastic mine detecting radar system using complex-valued self-organizing map that deals with multiple-frequency interferometric images,” *Neural Networks,* vol. 17, no. 8-9, pp. 1201-1210, 2004.

[8] Y. Nakano and A. Hirose, “Improvement of plastic landmine visualization performance by use of ring-CSOM and frequency-domain local correlation,” *IEICE Transactions on Electronics,* vol. E92.C, no. 1, pp. 102-108, 2009.

[9] T. Aoyagi, D. Radenamad, Y. Nakano, and A. Hirose, “Complex-valued self-organizing map clustering using complex inner product in active millimeter-wave imaging,” in *International Joint Conference on Neural Networks (IJCNN) 2010,* 2010, pp 1-6.

[10] F. Shang and A. Hirose, “Quaternion neural network-based PolSAR land classification in Poincare-sphere-parameter space,” *IEEE Transactions on Geoscience and Remote Sensing,* vol. 52, no. 9, pp. 5693–5703, 2014.

[11] F. Shang and A. Hirose, “Averaged Stokes vector based polarimetric SAR data interpretation,” *IEEE Transactions on Geoscience and Remote Sensing,* vol. 53, no. 8, pp. 4536–4547, 2015.

[12] K. Oyama and A. Hirose, “Phasor quaternion neural networks for singular point compensation in polarimetric-interferometric synthetic aperture radar,” *IEEE Transactions on Geoscience and Remote Sensing,* vol. 57, no. 5, pp. 2510–2519, 2019.

[13] Y. Song and A. Hirose, “Phasor-quaternion self-organizing-map-based ground penetrating radar systems,” *IEEE Transactions on Geoscience and Remote Sensing,* to appear 2021, 10.1109/TGRS.2021.3065137.

[14] Y. Song and A. Hirose, “Proposal of a ground penetrating radar system utilizing polarization information by using phasor-quaternion self-organizing map,” in *International Geoscience and Remote Sensing Symposium (IGARSS) 2021,* to be presented.

[15] Y. Nakano and A. Hirose, “Adaptive identification of landmine class by evaluating the total degree of conformity of ring-CSOM weights in a ground penetrating radar system,” *Australian Journal of Intelligent Information Processing Systems,* vol. 12, no. 1, pp. 23-28, 2010.